Mol Neurobiol (2017) 54:5928–5940
DOI 10.1007/s12035-016-0108-8

Pterostilbene Attenuates Early Brain Injury Following Subarachnoid Hemorrhage via Inhibition of the NLRP3 Inflammasome and Nox2-Related Oxidative Stress

Haixiao Liu[1] · Lei Zhao[1] · Liang Yue[1] · Bodong Wang[1] · Xia Li[1] · Hao Guo[1] · Yihui Ma[2] · Chen Yao[3] · Li Gao[1] · Jianping Deng[1] · Lihong Li[1] · Dayun Feng[1] · Yan Qu[1]

Received: 27 May 2016 / Accepted: 6 September 2016 / Published online: 24 September 2016

Abstract Pterostilbene (PTE), one of the polyphenols present in plants such as blueberries and grapes, has been suggested to have various effects, such as anti-oxidation, anti-apoptosis, and anti-cancer effects. Subarachnoid hemorrhage (SAH) is a severe neurological event known for its high morbidity and mortality. Recently, early brain injury (EBI) has been reported to play a significant role in the prognosis of patients with SAH. The present study aimed to investigate whether PTE could attenuate EBI after SAH was induced in C57BL/6 J mice. We also studied possible underlying mechanisms. After PTE treatment, the neurological score and brain water content of the mice were assessed. Oxidative stress and neuronal injury were also evaluated. Nucleotide-binding oligomerization domain-like receptor family pyrin domain-containing 3 (NLRP3) inflammasome activity was assessed using western blot analysis. Our results indicated that PTE treatment reduces the SAH grade, neurological score, and brain water content following SAH. PTE treatment also reduced NLRP3 inflammasome activation. PTE alleviated the oxidative stress following SAH as evidenced by the dihydroethidium staining, superoxide dismutase activity, malondialdehyde content, 3-nitrotyrosie and 8-hydroxy-2-deoxyguanosine levels, and $gp91^{phox}$ and 4-hydroxynonenal expression levels. Additionally, PTE treatment reduced neuronal apoptosis. In conclusion, our study suggests that PTE attenuates EBI following SAH possibly via the inhibition of NLRP3 inflammasome and Nox2-related oxidative stress.

Keywords Pterostilbene · Subarachnoid hemorrhage · Early brain injury · NLRP3 inflammasome · Oxidative stress · Nox2

Introduction

As a devastating cerebral vascular event, subarachnoid hemorrhage (SAH) is predominantly caused by ruptured aneurysm, arteriovenous malformation, hypertensive arteriosclerosis, abnormal vascular net at the base of the skull, or by violent trauma [1]. SAH is a serious condition because of its high morbidity and mortality rates [2, 3]. This complicated condition is intimately associated with a variety of physiological and pathological mechanisms, such as vasospasm, cerebral edema, obstructive hydrocephalus, diffuse/focal cerebral ischemia, or infarction [4, 5]. Recently, early brain injury (EBI) has been suggested to play a critical role in the prognosis of SAH. EBI refers to the immediate injury to the brain after SAH, before the onset of delayed vasospasm. Evidence shows that EBI, and not vasospasm, may be responsible for morbidity and mortality during the early 24–72 h after the SAH [6]. New therapeutics targeting the molecular mechanisms of EBI may be beneficial for improving patients' clinical outcomes. The mechanisms of oxidative stress, including reactive oxidative species (ROS) production, lipid peroxidation, protein inactivation, and DNA damage, cannot be ignored in early brain injury [7]. Nicotinamide adenine dinucleotide phosphate (NADPH) oxidases (Nox) are a family of enzymes that lead to the generation of ROS. It has been reported that $gp91^{phox}$ is the catalytic subunit of Nox2, and that

Haixiao Liu, Lei Zhao, and Liang Yue contributed equally to this work.

✉ Yan Qu
yanqu0123@fmmu.edu.cn

[1] Department of Neurosurgery, Tangdu Hospital, Fourth Military Medical University, Xi'an No. 1 Xinsi Road, Xi'an 710038, China

[2] Department of Neurosurgery, General Hospital of Lanzhou Military Area Command, Lanzhou 730050, China

[3] The Medical Machine Office, The 161 Hospital of PLA, Wuhan 430000, China

its activity is strongly associated with ROS production [8]. Additionally, increasing evidence indicates that inflammation has a pivotal role in the acute and chronic phases of neural injury caused by aneurysmal SAH [9]. Neuronal apoptosis is also an important therapeutic target for the attenuation of neural injury caused by aneurysmal SAH and has been successfully targeted in an animal model [10].

Notably, the nucleotide-binding oligomerization domain-like receptor family pyrin domain-containing 3 (NLRP3) inflammasome has been shown to play a critical role in the inflammatory response and to contribute to neuroinflammation after SAH [11]. The NLRP3 inflammasome consists of NOD-like receptor, NLRP3, apoptosis-associated speck-like protein containing caspase-1 activator domain (ASC), and caspase-1 [12]. Once activated, ASC and pro-caspase-1 are recruited, leading to caspase-1 activation, and subsequently, promotes the cleaving of pro-interleukin (IL)-1β and pro-IL-18 into their active forms. IL-1β and IL-18 can then induce neuroinflammation and neurodegeneration [13].

Pterostilbene (trans-3,5-dimethoxy-4-hydroxystilbene (PTE)) is an analog of resveratrol. They are both polyphenols produced by plant metabolism, which are common in the human diet. However, PTE has better oral bioavailability compared with resveratrol [14]. Research shows that these polyphenols have extensive protective effects on a serious of pathological states such as cancer and cardiovascular and neurodegenerative diseases [15, 16]. It is vitally important that PTE is able to pass the blood-brain barrier. Thus, oral or intraperitoneal administration of these plant-extracted stilbenes may be beneficial for the treatment of neuronal injury [17].

We have demonstrated that PTE treatment attenuates global cerebral ischemia-reperfusion (I/R) injury by reducing I/R-induced mitochondrial oxidative damage via the activation of hemeoxygenase (HO)-1 signaling [18]. However, the effects of PTE on EBI following SAH and the underlying mechanisms of these effects have not yet been reported. Therefore, this study aimed to determine whether PTE can reduce EBI after SAH, and if so, to investigate the possible underlying mechanisms.

Materials and Methods

Reagents

PTE, superoxide dismutase (SOD) assay kit, malondialdehyde (MDA) assay kit and ROS fluorescent probe-dihydroethidium (DHE), dimethyl sulfoxide (DMSO), and 4′,6-diamino-2-phenylindole (DAPI) were purchased from Sigma-Aldrich (St. Louis, MO, USA). Rabbit polyclonal antibody against $gp91^{phox}$ (ab80508), rabbit polyclonal antibody against 4-HNE (ab46545), rabbit polyclonal antibody against active caspase-3 (ab2302), and rabbit polyclonal antibody against interleukin-1β (IL-1β; ab9722) were obtained from Abcam (Cambridge, UK). Rabbit monoclonal antibody against Bcl-2 (no. 2870) rabbit monoclonal antibody against Bax (no. 14796) and rabbit monoclonal antibody against β-actin (no. 4970) were purchased from Cell Signaling Technology (Beverly, MA, USA). Rabbit polyclonal antibody against interleukin-18 (sc-7954), rabbit polyclonalan tibody against NLRP3 (sc-66846), rabbit polyclonal antibody against apoptosis-associated speck-like protein containing a caspase recruitment domain (ASC) (sc-22514-R), and goat polyclonal antibody against caspase-1 p20 (sc-1597) was purchased from Santa Cruz Biotechnology (Santa Cruz, CA, USA). Mouse monoclonal antibody against NeuN (MAB377) was purchased from Millipore (Billerica, MA, USA). Terminal deoxynucleotidyltransferased UTP nick-end labeling (TUNEL) kit was purchased from Roche (Mannheim, Germany). The ELISA kits for measuring 8-hydroxy-2-deoxyguanosine (8-OHdG) and 3-nitrotyrosine (3-NT) were purchased from Cell Biolabs (San Diego, USA). The HRP-conjugated rabbit anti-goat secondary antibody and HRP-conjugated goat anti-rabbit secondary antibody were purchased from Bioworld Co. (Shanghai, China). The Cy3-conjugated goat anti-mouse secondary antibody was purchased from the ComWin Biotech Co. (Beijing, China).

Animals

This study was performed according to the Guide for the Care and Use of Laboratory Animals, which is published by the US National Institutes of Health (National Institutes of Health Publication no. 85-23, revised 1996) and was approved by the Ethics Committee of the Fourth Military Medical University.

Healthy adult male C57BL/6 J mice weighing 20–25 g were used in our experiments. They were provided by the Animal Center of the Fourth Military Medical University. The mice were kept in a pathogen-free environment at a constant temperature (23 °C) and humidity (60 %), with a 12-h light-dark cycle and had free access to food and water.

SAH Model

We used the endovascular perforation subarachnoid hemorrhage model. The mice were anesthetized using 2 % pentobarbital sodium and then placed in the supine position. The mice's skin and then subcutaneous tissue along the midline of the neck were cut open to expose the left common carotid artery bifurcation. The left external carotid artery was ligated and dissected. A sharpened suture was inserted into the left internal carotid artery from the left external carotid artery stump. Resistance feeling is felt when piercing the artery at a point 10–12 mm inward from the common carotid artery bifurcation. At this point, we continued to insert 3 mm further to

perforate the bifurcation of the anterior and middle cerebral arteries. The suture remained in place for 20 s before withdrawal. Sham-operated mice underwent the same procedures, except for the 3 mm insertion.

Experimental Protocols

In this study, 197 mice were used and 22 mice were excluded because of the low SAH grades. The mice were randomly divided into a sham group (n = 36), an SAH group (n = 47), an SAH + vehicle group (n = 46), and an SAH + PTE group (n = 46). PTE was first dissolved in DMSO and then diluted in 0.9 % NaCl solution and was administered intraperitoneally twice (0.5 and 2 h after SAH induction) at a dose of 10 mg/(kg body weight). The SAH + vehicle group was administered the same volume of vehicle.

SAH Grade

According to the SAH grading scale reported previously [19], the severity of SAH was evaluated by an observer who was blind to the experimental groups. Twenty-four hours after SAH injury, the mice were re-anesthetized and killed, and their brains were removed immediately. We then rapidly recorded the high-resolution photos of the skull base to observe and analyze the circle of Willis and the basilar arteries. The basal cisterns were divided into six segments, each of which was evaluated by a blinded investigator, who graded them on a scale from 0 to 3 depending on the extent of subarachnoid blood clotting in the segment (Grade 0, no subarachnoid blood; grade 1, minimal subarachnoid blood; grade 2, moderate blood clot with recognizable arteries; grade3, blood clot obliterating all arteries within the segment). Mice with too mild (SAH grades ≤7 at 24 h) or too serious (death) of an injury were excluded from the groups.

Neurological Scores

In order to identify mice's sensorimotor deficits, neurological scores were blindly evaluated after 24 and 72 h according to the 18-point scoring system. This system includes six evaluating indicator (spontaneous activity, movements of all limbs, movements of forelimbs, climbing, reaction to touch on trunk, and vibrissae), each of which ranges from 0 to 3 points.

Brain Water Content

The animals were sacrificed under deep anesthesia after 24 or 72 h of the SAH surgery, then the brains were removed immediately and divided into four parts: left hemisphere, right hemisphere, cerebellum, and brain stem. After removal, each part was weighed immediately before being put into oven at the temperature from 95 to 100 °C for 72 h to get the wet weight. Then, weigh them once more after drying in the oven to obtain the dry weight. The percentage of tissue water content was calculated as ((wet weight − dry weight)/wet weight) × 100 %.

ROS Staining

Cellular ROS levels were analyzed using the ROS fluorescent probe DHE in images obtained with a laser confocal scanning microscope 24 h after SAH. Mice were transcardially perfused with 50 mL ice-cold 0.1 M phosphate-buffered saline (PBS; pH 7.4) after being anesthetized. The brains were quickly removed and frozen at −80 °C for 20 min, and soon after, they were sliced into 15-μm-thick coronal sections by suing a freezing microtome. The sections were then mounted onto polylysine-coated slides. After a 30-min incubation in DHE (10 μmol/L), the slices was observed and photographed using a microscope. The DHE-positive cells were counted to reflect the tissues' ROS levels, as well as their oxidative stress levels [20].

Measurement of MDA Levels and SOD Activities

The animals were killed 24 h following the SAH, and tissue homogenates were prepared for the detection of MDA levels and SOD activity. MDA levels were tested according to manufacturer instructions. The principle of this assay is that malondialdehyde and thiobarbituric acid react under acidic conditions and high temperature to generate red-brown 3,5,5'-threemethyloxazole-2,4-diketone, which has a maximum absorption peak at a wavelength of 532 nm. SOD activity was also determined following manufacturer instructions, which outline the WST-1 method. Changes in SOD activity were reflected by changes in absorbance at 550 nm [21, 22].

Evaluation of 3-NT and 8-OHdG Levels

The concentrations of 3-NT and 8-OHdG were measured according to the instructions of the manufacturer of a commercial enzyme-linked immunosorbent assay (ELISA) kit 24 h after the SAH. Briefly, samples, standards, and primary antibodies were added to the wells of a well plate, which was then incubated at 4 °C for 12 h. The samples were then incubated with a secondary antibody for 1 h at room temperature and a substrate solution for 15 min at room temperature in the dark. After adding the reaction terminating solution, the absorbance of contents of each well was measured and a standard curve was used to determine the levels of 3-NT and 8-OHdG in the samples [23].

TUNEL Staining

Cell apoptosis in the tissue was detected using terminal deoxynucleotidyl transferased UTP nick end labeling (TUNEL) staining 24 h after SAH induction. Mice were deeply anesthetized and transcardially perfused with 50 mL ice-cold 0.1 M PBS (pH 7.4) and then 60 mL 4 % paraformaldehyde (dissolved in PBS). The brains were immediately removed and fixed in the paraformaldehyde solution at 4 °C for 24 h. After dehydrating using sequential 24-h incubations in 10, 20, and 30 % sucrose solutions, the tissues were sliced. The slices were put in a humidified box, treated with 0.3 % hydrogen peroxide for 30 min at the room temperature and incubated with 0.25 % proteinase K for 45 min at 37 °C. The slices were then dyed using the TUNEL reaction solution (concentrated enzyme solution and labeling solution) prepared according to the manufacturer instructions in a humidified dark box for 60 min at 37 °C. Finally, the tissues were dyed using DAPI for 10 min at 37 °C. Each of these steps was followed by three 5-min PBS washes. Brain sections were covered using cover glasses and anti-fade mounting medium. The numbers of TUNEL-positive cells, representing apoptotic cells, and DAPI-stained cells, representing all cells, were separately counted in five fields randomly chosen under a high-power lens. The extent of cell apoptosis was evaluated by calculating the ratio of TUNEL-positive cells to DAPI-staining cells. This analysis was performed by a blinded observer.

NeuN Staining

For NeuN staining, the slices were incubated with 0.3 % hydrogen peroxide for 30 min at room temperature and treated with 0.15 % Triton X-100 for another 30 min at room temperature. The slices were then incubated with 10 % donkey serum for 45 min at room temperature, followed by incubation with a mouse anti-NeuN antibody overnight at 4 °C. Subsequently, the slices were incubated with Cy3-conjugated goat anti-mouse secondary antibody for 2 h at room temperature, and then stained with DAPI for 10 min at 37 °C. The survival rates of neurons were reflected by the proportions of NeuN-positive cells.

Western Blot

The left basal cortical samples were homogenized using an ultrasonic homogenizer in a mixture of lysis buffer and 1 % protease inhibitor for western blotting. The lysates were centrifuged, and the resulting supernatant was transferred to a new tube and stored at −80 °C. Protein concentrations were measured using bicinchoninic acid (BCA) by using an enhanced BCA protein assay kit. Protein samples were loaded onto a 10–15 % sodium dodecyl sulfate (SDS)-polyacrylamide gel, separated by electrophoresis, and electrophoretically transferred to polyvinylidene fluoride (PVDF) membranes, which were pre-activated by methanol. The PVDF membranes were blocked in 5 % evaporated skimmed milk diluted in Tris-buffered saline containing Tween-20 (TBST) for 1 h at room temperature. The membranes were subsequently incubated with primary antibodies against $gp91^{phox}$, 4-HNE, Bcl-2, Bax, active caspase-3, NLRP3, ASC, caspase-1, p20, IL-1β, IL-18, and β-actin at 4 °C overnight. They were then incubated with appropriate secondary antibodies at room temperature for 2 h. The antibody incubations were followed by three 5-min TBST washes. The protein bands were detected and quantified by the Bio-Rad imaging system (Bio-Rad, Hercules, CA, USA).

Statistical Analysis

GraphPad Prism5 software (LaJolla, CA, USA) was used to analyze the data in our study. Data for SAH grades and neurological scores are expressed as median and 25th to 75th percentiles and were analyzed using the Mann-Whitney *U* test or Kruskal-Wallis one-way analysis of variance (ANOVA) on ranks, followed by Dunn's or Tukey's post hoc analysis. Other data are expressed as mean ± standard deviation (SD). Fisher's exact test was used for mortality analysis. One-way ANOVA followed by Bonferroni multiple comparisons test was used for intergroup comparisons. Data were considered statistically significant if P was <0.05.

Results

The Mortality and SAH Grade in Each Group

None of the animals in the sham group died. The mortalities of the SAH, SAH + vehicle, and SAH + PTE group were 23.4 % (11 of 47 mice), 21.7 % (10 of 46 mice), and 21.7 % (10 of 46 mice), respectively (Fig. 1a). The SAH grades of the animals were evaluated after they were killed. Blood clots were clearly visible around the circle of Willis and the ventral brainstem of the mice in the SAH, SAH + vehicle, and SAH + PTE groups. The differences between these groups' scores were of no statistical significance (Fig. 1b).

Effects of PTE on Neurological Score and Brain Water Content

The neurological scores of each group were measured 24 and 72 h after the SAH. Brain water content in the left hemisphere, the right hemisphere, the cerebellum, and the brain stem were tested separately at the same time points. Neurological scores decreased dramatically and brain

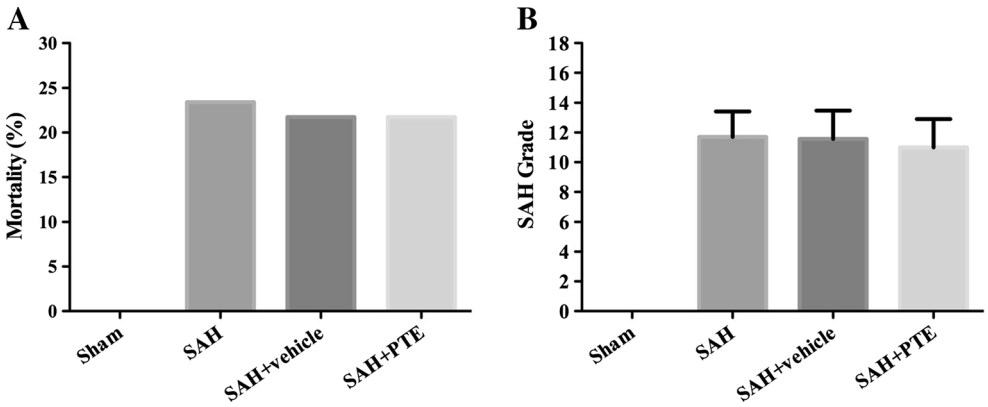

Fig. 1 Mortality and SAH grades in each group. **a** Mortalities in the sham, SAH, SAH + vehicle, and SAH + PTE groups were 0 %, 23.4 % (11 of 47 mice), 21.7 % (10 of 46 mice), and 21.7 % (10 of 46 mice), respectively. **b** SAH grades in each group. Values for SAH grades are represented as median and 25th to 75th percentiles

water content increased significantly after SAH (vs. the sham group, $P < 0.05$) (Fig. 2). However, the difference between the SAH and SAH + vehicle groups was of no statistical significance. PTE administration alleviated the neurological deficits following SAH injury and decreased brain water content in the left hemisphere, which was the ipsilateral side to the injury (vs. the SAH + vehicle group, $P < 0.05$) (Fig. 2).

PTE Treatment Attenuates Oxidative Stress Following SAH

We evaluated the effects of PTE treatment on oxidative stress 24 h after SAH induction. Our results suggest that PTE has a protective effect against oxidative stress after SAH. DHE-staining results were recorded using confocal microscopy. Statistics revealed that the numbers of DHE-positive cells in

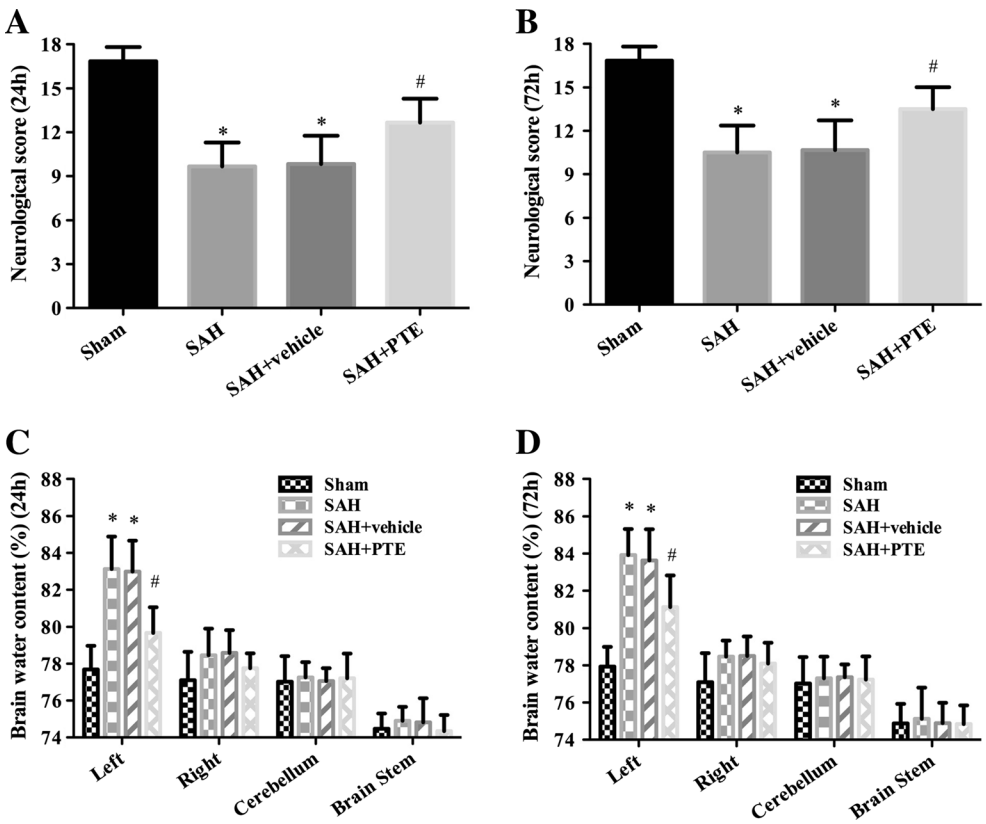

Fig. 2 Effects of PTE on neurological score and brain water content 24 and 72 h after SAH. **a**, **b** Neurological scores 24 and 72 h after SAH indicate that the difference between the SAH and SAH + vehicle groups had no significance. However, the neurological scores of the SAH + PTE group are higher than those of the SAH + vehicle group. **c**, **d** Brain water content of the left hemisphere, the right hemisphere, the cerebellum, and the brainstem were tested separately 24 and 72 h after SAH. The injury was on the left side. The data from the SAH and SAH + vehicle groups did not indicate statistically significant differences. However, the brain water content of the SAH + PTE group is lower than that of the SAH + vehicle group. Values for neurological scores are represented as median and 25th to 75th percentiles. Values for brain water contents are represented as mean ± SD, $n = 6$ for each group. $^{*}P < 0.05$ vs. sham group; $^{\#}P < 0.05$ vs. SAH + vehicle group

the SAH + PTE group were significantly decreased (vs. the SAH + vehicle group, $P < 0.05$) (Fig. 3a, b). Our data indicated that MDA levels were statistically lower in the SAH + PTE group (vs. the SAH + vehicle group, $P < 0.05$) (Fig. 3c), while the difference between the SAH and SAH + vehicle groups had no significance. The group treated with PTE had higher SOD activity (vs. the SAH + vehicle group, $P < 0.05$) (Fig. 3d). The levels of 3-NT and 8-OHdG, which are markers of protein and DNA damage, respectively, increased significantly in the SAH group (vs. the sham group, $P < 0.05$). PTE treatment induced dramatic decreases of the levels of 3-NT and 8-OHdG (vs. the SAH + vehicle group, $P < 0.05$) (Fig. 3e, f). Like MDA, 4-HNE is a lipid peroxide, which is produced in the presence of ROS. $gp91^{phox}$ is a catalytic subunit of Nox2. Western blotting was performed to determine the effects of PTE on the expression levels of $gp91^{phox}$ and 4-HNE. The SAH group had significant increases in the expression levels of $gp91^{phox}$ and 4-HNE (vs. the sham group, $P < 0.05$), while the increases of these levels in SAH + PTE group were less dramatic (vs. the SAH + vehicle group, $P < 0.05$) (Fig. 3g–i). These results indicate that PTE attenuates EBI following SAH via the inhibition of Nox2-related oxidative stress.

PTE Treatment Attenuates Neuronal Death Following SAH

We quantified cellular death by using TUNEL staining and NeuN immunofluorescence staining 24 h after SAH induction. Our results indicated that the apoptotic index was significantly increased in the SAH group (vs. the sham group, $P < 0.05$), while the difference between the SAH and SAH + vehicle groups had no statistical significance. The administration of PTE distinctively decreased apoptosis (vs. the SAH + vehicle group, $P < 0.05$) (Fig. 4a, c). NeuN staining was performed to quantify the cell survival rate. The numbers of NeuN-positive cells, which were decreased by SAH injury,

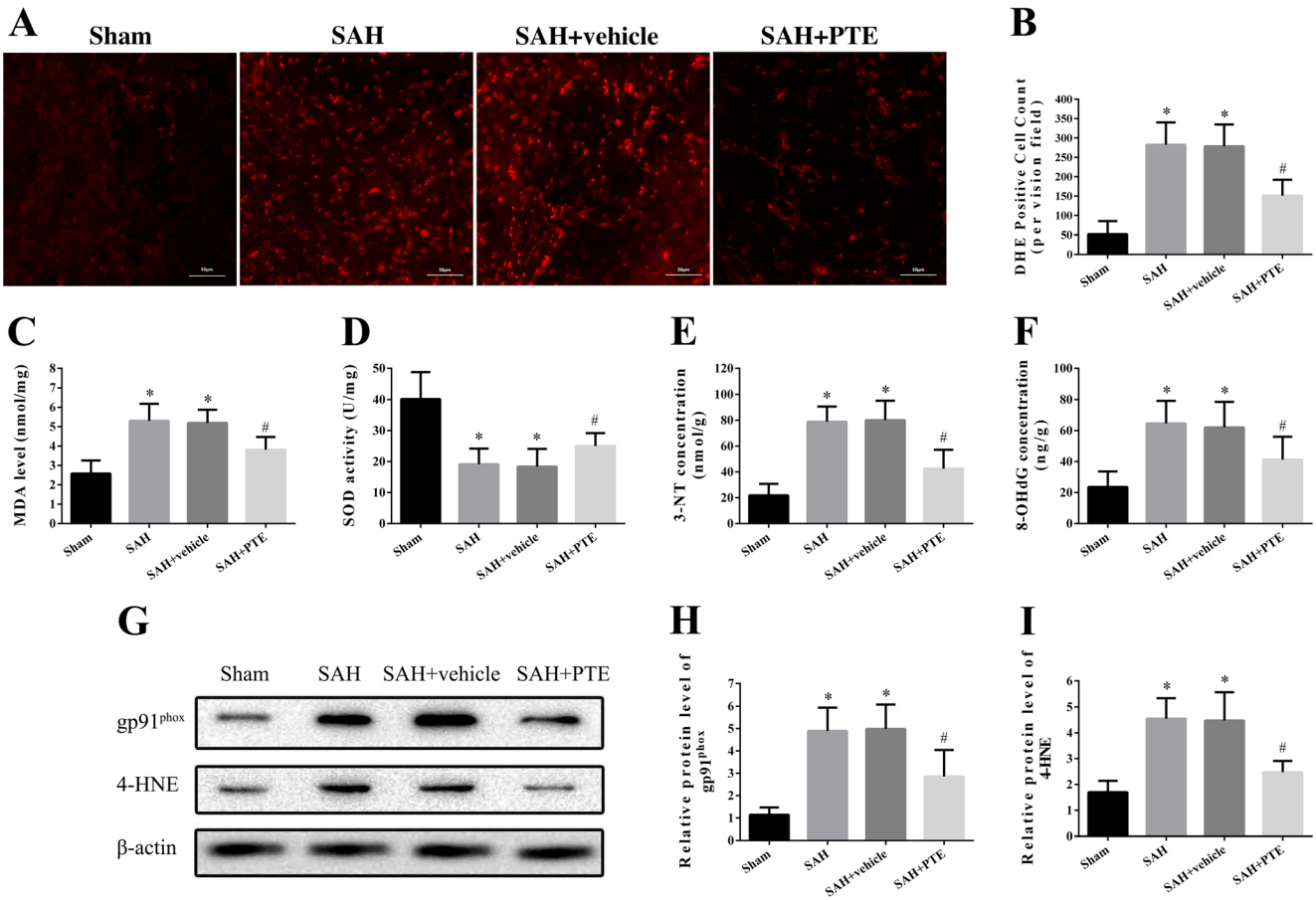

Fig. 3 Effects of PTE treatment on oxidative stress 24 h after SAH induction. **a** Representative confocal images of DHE staining are shown. *Scale bar* = 50 μm. **b** The histogram shows the percentages of DHE-positive cells. **c** MDA levels. **d** SOD activity. **e** 3-NT concentration. **f** 8-OHdG concentration. **g** The expression levels of $gp91^{phox}$ and 4-HNE as detected by western blot. **h** The relative levels of $gp91^{phox}$. **i** The relative levels of 4-HNE. Values are represented as mean ± SD, $n = 6$ for each group. $^{*}P < 0.05$ vs. sham group; $^{\#}P < 0.05$ vs. SAH + vehicle group

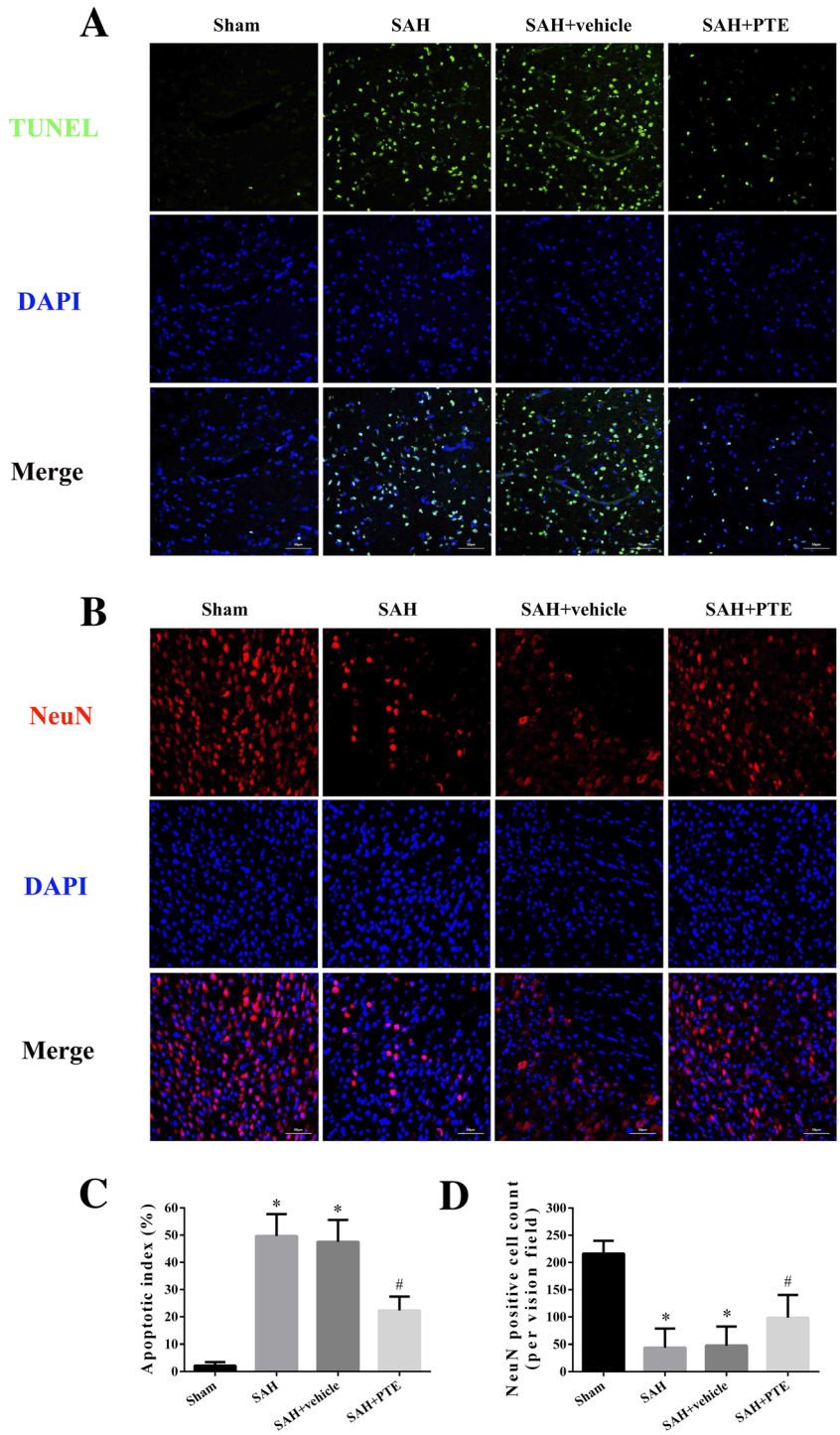

Fig. 4 Effects of PTE treatment on neuronal death 24 h after SAH induction. **a** Representative images of TUNEL staining. **b** Representative images of NeuN staining and **c**, **d** histograms show the quantification of TUNEL- and NeuN-positive cells. Values are represented as mean ± SD, $n = 6$ for each group. $^{*}P < 0.05$ vs. sham group; $^{\#}P < 0.05$ vs. SAH + vehicle group

were increased in the SAH + PTE group (vs. the SAH + vehicle group, $P < 0.05$) (Fig. 4b, d).

Effects of PTE Treatment on Apoptosis Signaling Following SAH

Western blotting was used to detect the expression levels of Bcl-2, Bax, and active caspase-3 24 h after SAH induction. As shown in Fig. 5, our results revealed significant up-regulation in the expression levels of Bax and activated caspase-3 after SAH (vs. the sham group, $P < 0.05$). However, this phenomenon was partially offset by PTE. The expression of Bcl-2 was lower in SAH and the SAH + vehicle groups compared with the sham group, and the expression levels of Bcl-2 increased notably in the SAH + PTE group (vs. the SAH + vehicle group, $P < 0.05$).

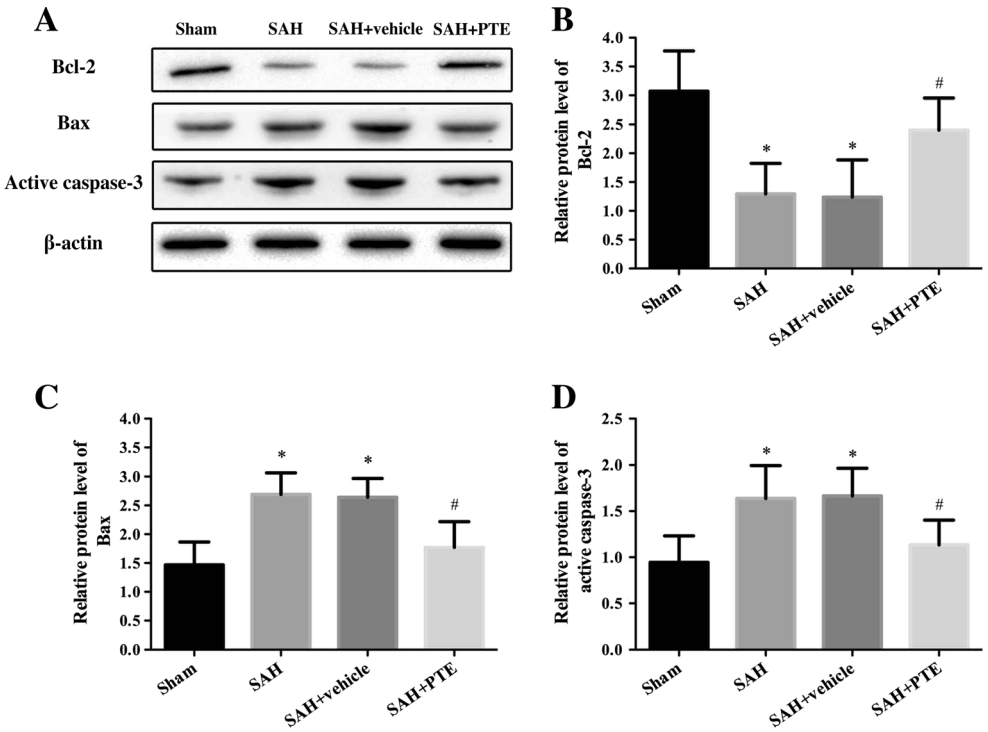

Fig. 5 Effects of PTE on the expression levels of Bcl-2, Bax, and active caspase-3 24 h after SAH, as detected by western blot. **a** Representative western blot images. **b** Bcl-2 levels. **c** Bax levels. **d** Active caspase-3 levels. Values are represented as mean ± SD, $n = 6$ for each group. $^{*}P < 0.05$ vs. sham group; $^{\#}P < 0.05$ vs. SAH + vehicle group

Effects of PTE Treatment on the NLRP3 Inflammasome Following SAH

Western blotting was performed to investigate whether PTE treatment reduced NLRP3 inflammasome activation 24 h after SAH induction. The expression levels of NLRP3, ASC, caspase-1 p20, IL-1β, and IL-18 were measured and analyzed (Fig. 6). The protein level of NLRP3, ASC, active caspase-1, IL-1β, and IL-18 increased markedly in brain tissues after the SAH (vs. the sham group, $P < 0.05$). However, the levels of these proteins did not show significant difference between the SAH and SAH + vehicle groups. PTE administration significantly reduced the expression levels of NLRP3, ASC, active aspase-1, IL-1β, and IL-18.

Discussion

The major findings of the present study are: (1) PTE treatment alleviates neurological deficits and brain edema after SAH. (2) PTE treatment inhibits NLRP3 inflammasome activation after SAH. (3) PTE treatmentreduces Nox2-related oxidative stress following SAH. PTE treatment alleviates the animals' neurological deficits and brain edema 24 and 72 h after SAH induction. Moreover, the numbers of DHE-positive cells, which represent reactive oxygen species production, were lower in SAH + PTE group than in the SAH and SAH + vehicle groups. The reductions in MDA, 3-NT, 8-OHdG, $gp91^{phox}$, and 4-HNE levels and the elevation in SOD activity also reflect PTE's persistent effects in alleviating oxidative stress following SAH. PTE can also decrease neuronal apoptosis. In addition, the activation of the NLRP3 inflammasome can be observed in the tissue, following SAH, and is inhibited by PTE treatment.

EBI is regarded as the critical cause of high mortality andmorbidity following SAH, as well as the major therapeutic target in the management of SAH [24, 25]. Increased intracranial pressure (ICP), decreased cerebral blood flow (CBF), and global cerebral ischemia are critical causative factors during the EBI period. These events induce the pathologic secondary injury processes of blood-brain barrier disruption, inflammation, the oxidative cascades, and ultimately lead to cell apoptosis and death [3, 26, 27]. Various molecular mechanisms have been shown to participate in the pathophysiology of EBI, including inflammation, oxidative stress, and cell apoptosis. These mechanisms are thought to be involved in the etiology of EBI and are potential targets for therapeutic intervention [28].

PTE is a dimethylated analog of resveratrol with higher bioavailability. It is found in plants such as blueberries, grapes, and *Pterocarpus marsupium* [29]. Research has indicated that resveratrol has comprehensive protective effects, including protection against the amplification and metastasis of tumor cells, cardiovascular dysfunction, stroke-associated brain damage, and neurodegenerative disease. It is also known to delay aging and lead to weight loss [29, 30]. Although much study has focused on the beneficial effects of resveratrol and other stilbenes for a long time, the beneficial effects of stilbenes on the central nervous system has only received attention in recent years [31]. Rimando et al. first reported that the peroxyl-radical scavenging activity of PTE was similar to that

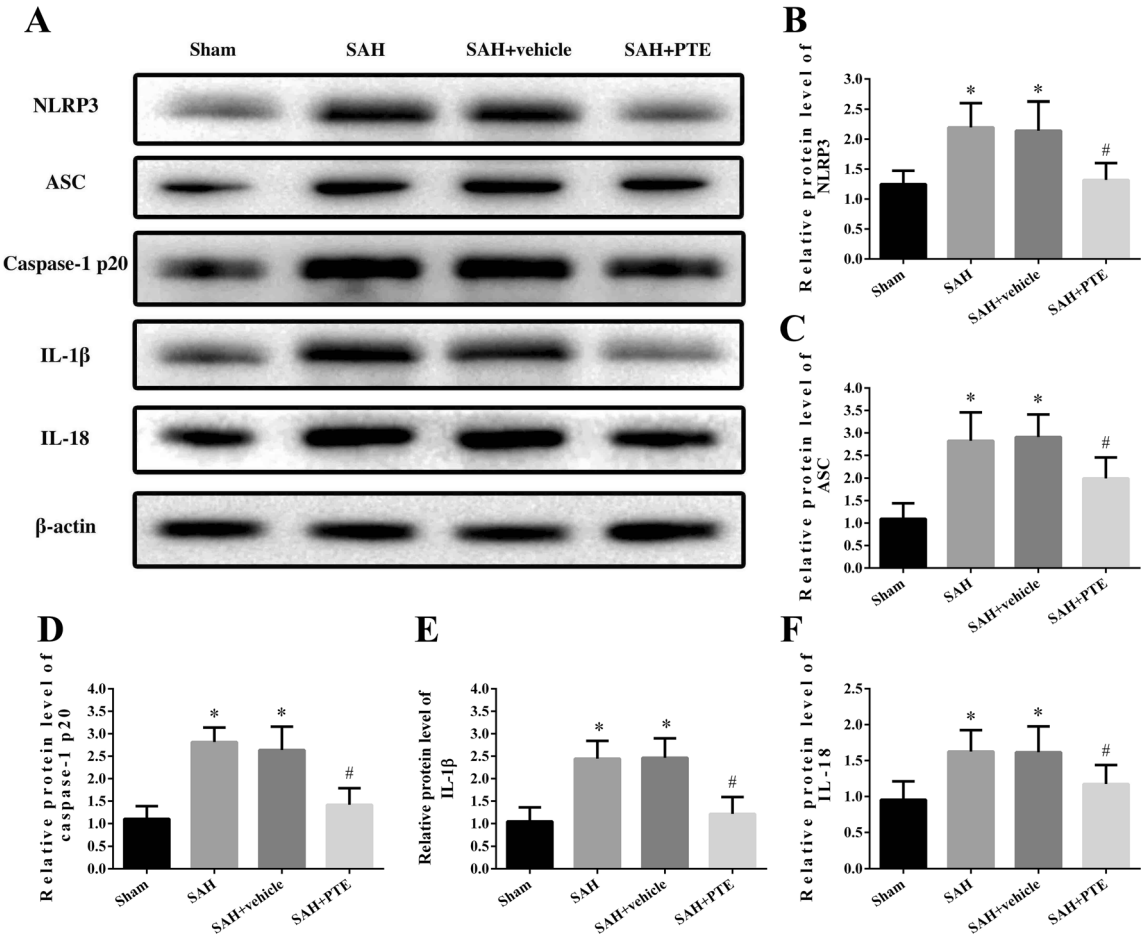

Fig. 6 Effects of PTE treatment on the NLRP3 inflammasome activation 24 h after SAH. **a** Representative western blot images. **b** NLRP3 levels. **c** ASC levels. **d** Caspase-1 p20 levels. **e** IL-1β levels. **f** IL-18 levels. Values are represented as mean ± SD, $n = 6$ for each group. $^{*}P < 0.05$ vs. sham group; $^{\#}P < 0.05$ vs. SAH + vehicle group

of resveratrol [32]. This effect of reducing oxidative stress is achieved directly by chemical reactions mediated by polyphenols, but more importantly, is indirectly achieved by regulating transcriptional factors, such as NF-κB, AP-1, FoxOs, Nrf2/Keap1, as well as by changing nuclear histone acetylation [33, 34]. PTE's anti-oxidant, anti-apoptosis, and anti-cancer properties have extensive biological effects in multiple organs and tissues such as breasts, the cardiovascular system, the alimentary system, the hematological system, and the prostate, as well as in metabolism [29].

PTE also has protective effects in neurons. These effects are known to originate from PTE's powerful anti-oxidant and anti-inflammation properties. These effects act through complicated mechanisms, such as the inhibition of ROS production, up-regulation of levels of PPAR-α levels, induction of MnSOD, down-regulation of levels of phosphorylated JNK and tau levels, suppression of the expression of iNOS and COX-2 expression, activation of the SIRT1 pathway, and inhibition of MAPK signal transduction pathway, which all suppress the activation ofthe NF-κB signaling pathway [16, 29, 31, 35]. Previous studies have also shown that PTE suppresses miR-377 to up-regulate SOD and inhibit the activation of the NLRP3 inflammasome pathway and alleviates oxidative stress and inflammation [36].

Our previous work demonstrated in the cerebral ischemia reperfusion mice model that PTE significantly attenuates the mitochondrial oxidative damage through regulating the mitochondrial cytochrome *c* release and the production of ROS [18]. This study showed that the most important therapeutic target of PTE on SAH might be the inhibition of the activity of NOX-2 and the release of ROS.

It has been reported that $gp91^{phox}$ is the catalytic subunit of Nox2 [37]. Together with its homologs of Nox1, Nox3, Nox4, Nox5, Duox1, and Duox2, Nox2 is an important member of the NOX family. The substrates of NADPH oxidase include ROS, which play significant roles in a range of diseases as signaling molecules regulating cell differentiation, proliferation, aging, apoptosis, and other cellular activities [38, 39]. In

this study, the expression of $gp91^{phox}$ together with ROS production induced by SAH is suppressed significantly by PTE, which is vital and cannot be ignored.

Oxygen-free radicals not only induce cell damage by inducing the peroxidation of polyunsaturated fatty acids on the biological membranes but also by decomposing these products. The amounts of 3-NT and MDA often reflect the degree of lipid peroxidation in tissue and thus indirectly reflect the degree of cell damage [40]. Peroxidation processes take place at the side chains of polyunsaturated fatty acids in biological membranes (phospholipids, enzymes, and membrane receptors), and in nucleic acids and other macromolecules. Peroxidation thus changes the fluidity and permeability of the cell membrane, and ultimately destroys cell structure and function.

SOD is an important anti-oxidant enzyme in organisms, catalyzes the dismutation of superoxide anion, and generates hydrogen peroxide (H_2O_2) and oxygen (O_2). The activity of SOD indirectly reflects the ability of the cell to clear oxyradicals [22]. 8-OHDG is one of the most sensitive DNA damage markers and is produced following hydroxyl radical induction during oxidative stress. 8-OHdG lesions can be eliminated by DNA repair enzymes, but they can also cause permanent changes in DNA structure if they are not excised [41]. Detection of changes in these biochemical indicators is a reflection of PTE's comprehensive effects in alleviating oxidative stress in EBI after SAH induction.

As is well known, neuroinflammation mediates the injury expansion and behavioral deficits [42, 43]. Peripheral immune cells are recruited to and activated in the damaged brain areas and release inflammatory cytokines in the cerebral parenchyma [44].

The NLRP3 inflammasome has been reported to take part in the pathogenesis of central nervous system disorders, such as ischemic stroke [45], intracranial hemorrhage [46], traumatic brain injury [47], and meningitis [48]. The NLRP3 inflammasome, which is associated with ASC and caspase protease, can recruit and activate caspase-1 and therefore induces the cleavage and maturation of pro-IL-1β and pro-IL-18 [49].

In this study, we proved that the installation and activation of NLRP3 inflammasome can be inhibited by PTE administration, which indicated that the protective effects of it also originate from the powerful anti-inflammation properties.

The activation of the NLRP3 inflammasome accelerates the process of inflammation and apoptosis and promotes oxidative stress-associated ROS generation [50, 51]. Cell apoptosis can be remarkably alleviated by inhibiting the activation of the NLRP3 inflammasome [52]. Interestingly, ROS can increase p38 MAPK phosphorylation while promoting the activation of the NLRP3 inflammasome. It can also increase the expression of thioredoxin-interacting protein (TXNIP) expression, which binds with thioredoxin (Trx), thus counteracting its suppression to NLRP3 inflammasome [46, 53, 54]. Pore formation, potassium (K^+) efflux, and lysosomal destabilization and rupture are associated with NLRP3 activation [49, 55]. The NLRP3 inflammasome has been suggested to be responsible for brain injury following SAH [11, 56].

The inflammatory factors released into microenvironment, such as IL-1β and TNF-α, will accelerate the Ca2+ influx and exitotoxicity of neurons through binding to their receptors on the membrane. As a result, the dysfunctions of mitochondrial lead to the decrease of ATP and the production and release of ROS. The energy failure and oxidative stress start up cellular apoptosis [57–59].

The members of Bcl-2 family play important parts in cellular apoptosis [60]. This protein family can be divided into two categories according to their molecular biological effects: the members of anti-apoptosis group include Bcl-2, Bcl-XL, Bcl-W, etc., and the members of pro-apoptosis group includes Bax, Bak, Bad, etc. [56, 61]. Bcl-2 is localized to the outer membrane of mitochondria, where it plays an important role in promoting cellular survival and inhibiting the actions of pro-apoptotic proteins. The pro-apoptotic members, such as Bcl-2-associated X protein (Bax), and Bcl-2 homologous antagonist killer (Bak), normally act on the mitochondrial membrane to promote permeabilization and release of cytochrome *c* and ROS, which are important signals in the apoptosis cascade [62].

Bcl-2 can combine with the other proteins in Bcl-2 family to form dimer. The dimer formed by Bcl-2 and Bax can regulate the apoptosis in cell. The Bax/Bax homo-dimers will form if Bax keeps on a higher level than Bcl-2, which promotes cell death. On the contrary, if the relative amount of Bcl-2 is higher than that of Bax, more Bcl-2/Bax heterodimers will replace Bax/Bax homo-dimers in cell, thus inhibits the cell death. Meanwhile, the amount of Bcl-2/Bcl-2 homodimers will form in this case, which acts as cell death inhibitors. Dephosphorylated BAD, which belongs to the BH3-only subfamily of Bcl-2 family, can form heterodimer with Bcl-2 and Bcl-xL, and thus allowing Bax to trigger apoptosis [63, 64]. When phosphorylated by Akt, BAD forms protein dimer, and leaves Bcl-2 free to inhibit Bax-triggered apoptosis [65].

Bcl-2 can also inhibit cellular apoptosis through other mechanisms. Over-expression of Bcl-2 can reduce the generation of oxygen free radicals and the formation of lipid peroxide, thus scavenge the reactive oxygen species in cell indirectly [66]. The release of cytochrome *c* (Cyt *c*), which may block the transport of electron in the respiratory chain and result in the accumulation of superoxide anion, can also be inhibited by Bcl-2 [67]. Besides, Bcl-2 can up-regulate the level and the activity of glutathione (GSH), inhibit the release of AIF into cytoplasm, and regulate the transmembrance flow of Ca^{2+} [68]. On the contrary, Bax and Bak are believed to initiate apoptosis by forming a pore in the mitochondrial outer membrane that allows cytochrome *c* to escape into the cytoplasm and activate the pro-apoptotic caspase cascade [62]. Bcl-2 and Bax are both pivotal apoptosis-related molecular in mitochondria and

antagonize each other to keep balance, which would break in the pathological conditions. This study shows that PTE can alleviate apoptosis caused by EBI through the Bcl-2 up-regulating and Bax/caspase cascade inhibiting mechanism.

In addition, evidence also suggests that the phosphoinositide 3-kinase (PI3K)/Akt pathway plays an important neuroprotective role in apoptosis after SAH. PI3K can be activated by growth factors, and then catalyzes the phosphorylation of PIP2 and generates PIP3, which would activate the 3′-phosphoinositide-dependent kinase (PDK). The activated PDK activates Akt. As an inhibitor to apoptosis, phosphorylated Akt inactivates its downstream targets, such as Bcl2-associated agonist of cell death, glycogen synthase kinase 3 and caspase-3 [69, 10, 70].

In this study, we have detected the total protein expression level and the phosphorylation level of Akt to investigate whether Akt pathway takes part in the protective effect of PTE. The current data of western blot did not show significant changes on the phosphorylation level of Akt. Taking the limitation of technologies and the deviations of experiments into consideration, we could not draw the conclusion whether Akt pathway takes part in the protective effect of PTE till now. And further research based on the expansion of sample size and the change of experimental conditions is still needed.

The current situation of SAH treatment is that most therapies aim at the primary injury, such as the removal of aneurysm by interventional operation, and the treatment to improve symptoms including the control of intracranial pressure, blood pressure, plasma osmotic pressure, and body temperature [71]. While, the methods to wipe off EBI through blocking or weakening the oxidative stress, inflammation, and apoptosis are novel treatment concepts and have not been widely used. So, this study might be enlightening, in a manner, and a fresh impetus to improve the prognosis of subarachnoid hemorrhage patients [72].

In summary, the present study demonstrates that PTE alleviates EBI following SAH via the inhibition of NLRP3 inflammasome activation and Nox2-related oxidative stress. Our findings suggest the possible therapeutic application of PTE for the treatment of SAH. But the underlying mechanisms and the relationship between them must be made clearer before clinical use.

Acknowledgments This work was supported by grants from the National Natural Science Foundation of China (81571215, 81630027, 81401020) and Leading Talents of Middle Age and Young in S & T Innovation supported by the Chinese Science and Technology Ministry (2013RA2181).

Compliance with Ethical Standards

Conflict of Interest The authors have declared that no competing interests exist.

References

1. Sehba FA, Hou J, Pluta RM, Zhang JH (2012) The importance of early brain injury after subarachnoid hemorrhage. Prog Neurobiol 97(1):14–37. doi:10.1016/j.pneurobio.2012.02.003
2. Bing Z, Rabinstein AA, Murad MH, Lanzino G, Panni P, Brinjikji W (2015) Surgical and endovascular treatment of poor-grade aneurysmal subarachnoid hemorrhage: a systematic review and meta-analysis. J Neurosurg Sci
3. Nogueira AB, Nogueira AB, Esteves Veiga JC, Teixeira MJ (2014) Multimodality monitoring, inflammation, and neuroregeneration in subarachnoid hemorrhage. Neurosurgery 75(6):678–689. doi:10.1227/NEU.0000000000000512
4. Chen S, Feng H, Sherchan P, Klebe D, Zhao G, Sun X, Zhang J, Tang J, Zhang JH (2014) Controversies and evolving new mechanisms in subarachnoid hemorrhage. Prog Neurobiol 115:64–91. doi:10.1016/j.pneurobio.2013.09.002
5. Dreier JP, Drenckhahn C, Woitzik J, Major S, Offenhauser N, Weber-Carstens S, Wolf S, Strong AJ, Vajkoczy P, Hartings JA, Group CS (2013) Spreading ischemia after aneurysmal subarachnoid hemorrhage. Acta Neurochir Suppl 115:125–129. doi:10.1007/978-3-7091-1192-5_26
6. Helbok R, Schiefecker AJ, Beer R, Dietmann A, Antunes AP, Sohm F, Fischer M, Hackl WO, Rhomberg P, Lackner P, Pfausler B, Thome C, Humpel C, Schmutzhard E (2015) Early brain injury after aneurysmal subarachnoid hemorrhage: a multimodal neuromonitoring study. Crit Care 19:75. doi:10.1186/s13054-015-0809-9
7. Echigo R, Shimohata N, Karatsu K, Yano F, Kayasuga-Kariya Y, Fujisawa A, Ohto T, Kita Y, Nakamura M, Suzuki S, Mochizuki M, Shimizu T, Chung UI, Sasaki N (2012) Trehalose treatment suppresses inflammation, oxidative stress, and vasospasm induced by experimental subarachnoid hemorrhage. J Transl Med 10:80. doi:10.1186/1479-5876-10-80
8. Hernandes MS, D'Avila JC, Trevelin SC, Reis PA, Kinjo ER, Lopes LR, Castro-Faria-Neto HC, Cunha FQ, Britto LR, Bozza FA (2014) The role of Nox2-derived ROS in the development of cognitive impairment after sepsis. J Neuroinflammation 11:36. doi:10.1186/1742-2094-11-36
9. Lucke-Wold BP, Logsdon AF, Manoranjan B, Turner RC, McConnell E, Vates GE, Huber JD, Rosen CL, Simard JM (2016) Aneurysmal subarachnoid hemorrhage and neuroinflammation: a comprehensive review. Int J Mol Sci 17(4). doi:10.3390/ijms17040497
10. Zhao L, Liu H, Yue L, Zhang J, Li X, Wang B, Lin Y, Qu Y (2016) Melatonin attenuates early brain injury via the melatonin receptor/Sirt1/NF-kappaB signaling pathway following subarachnoid hemorrhage in mice. Mol Neurobiol. doi:10.1007/s12035-016-9776-7
11. Shao A, Wu H, Hong Y, Tu S, Sun X, Wu Q, Zhao Q, Zhang J, Sheng J (2015) Hydrogen-rich saline attenuated subarachnoid hemorrhage-induced early brain injury in rats by suppressing inflammatory response: possible involvement of NF-kappaB pathway and NLRP3 inflammasome. Mol Neurobiol. doi:10.1007/s12035-015-9242-y
12. Lamkanfi M, Dixit VM (2011) Modulation of inflammasome pathways by bacterial and viral pathogens. J Immunol 187(2):597–602. doi:10.4049/jimmunol.1100229
13. Felderhoff-Mueser U, Schmidt OI, Oberholzer A, Buhrer C, Stahel PF (2005) IL-18: a key player in neuroinflammation and neurodegeneration? Trends Neurosci 28(9):487–493. doi:10.1016/j.tins.2005.06.008
14. Kapetanovic IM, Muzzio M, Huang Z, Thompson TN, McCormick DL (2011) Pharmacokinetics, oral bioavailability, and metabolic profile of resveratrol and its dimethylether analog, pterostilbene, in rats.

Cancer Chemother Pharmacol 68(3):593–601. doi:10.1007/s00280-010-1525-4
15. Estrela JM, Ortega A, Mena S, Rodriguez ML, Asensi M (2013) Pterostilbene: Biomedical applications. Crit Rev Clin Lab Sci 50(3):65–78. doi:10.3109/10408363.2013.805182
16. Nikhil K, Sharan S, Palla SR, Sondhi SM, Peddinti RK, Roy P (2015) Understanding the mode of action of a pterostilbene derivative as anti-inflammatory agent. Int Immunopharmacol 28(1):10–21. doi:10.1016/j.intimp.2015.05.003
17. Huynh TT, Lin CM, Lee WH, Wu AT, Lin YK, Lin YF, Yeh CT, Wang LS (2015) Pterostilbene suppressed irradiation-resistant glioma stem cells by modulating GRP78/miR-205 axis. J Nutr Biochem 26(5):466–475. doi:10.1016/j.jnutbio.2014.11.015
18. Yang Y, Wang J, Li Y, Fan C, Jiang S, Zhao L, Di S, Xin Z, Wang B, Wu G, Li X, Li Z, Gao X, Dong Y, Qu Y (2015) HO-1 signaling activation by pterostilbene treatment attenuates mitochondrial oxidative damage induced by cerebral ischemia reperfusion injury. Mol Neurobiol. doi:10.1007/s12035-015-9194-2
19. Sugawara T, Ayer R, Jadhav V, Zhang JH (2008) A new grading system evaluating bleeding scale in filament perforation subarachnoid hemorrhage rat model. J Neurosci Methods 167(2):327–334. doi:10.1016/j.jneumeth.2007.08.004
20. Yan H, Zhang D, Hao S, Li K, Hang CH (2015) Role of mitochondrial calcium uniporter in early brain injury after experimental subarachnoid hemorrhage. Mol Neurobiol 52(3):1637–1647. doi:10.1007/s12035-014-8942-z
21. Zhang XS, Zhang X, Zhou ML, Zhou XM, Li N, Li W, Cong ZX, Sun Q, Zhuang Z, Wang CX, Shi JX (2014) Amelioration of oxidative stress and protection against early brain injury by astaxanthin after experimental subarachnoid hemorrhage. J Neurosurg 121(1):42–54. doi:10.3171/2014.2.JNS13730
22. Cai J, Cao S, Chen J, Yan F, Chen G, Dai Y (2015) Progesterone alleviates acute brain injury via reducing apoptosis and oxidative stress in a rat experimental subarachnoid hemorrhage model. Neurosci Lett 600:238–243. doi:10.1016/j.neulet.2015.06.023
23. Pylvas M, Puistola U, Laatio L, Kauppila S, Karihtala P (2011) Elevated serum 8-OHdG is associated with poor prognosis in epithelial ovarian cancer. Anticancer Res 31(4):1411–1415
24. Bederson JB, Connolly ES Jr, Batjer HH, Dacey RG, Dion JE, Diringer MN, Duldner JE Jr, Harbaugh RE, Patel AB, Rosenwasser RH, American Heart A (2009) Guidelines for the management of aneurysmal subarachnoid hemorrhage: a statement for healthcare professionals from a special writing group of the stroke council, American Heart Association. Stroke; a journal of cerebral circulation 40(3):994–1025. doi:10.1161/STROKEAHA.108.191395
25. Broderick JP, Brott TG, Duldner JE, Tomsick T, Leach A (1994) Initial and recurrent bleeding are the major causes of death following subarachnoid hemorrhage. Stroke; J Cereb Circ 25(7):1342–1347
26. Fujii M, Yan J, Rolland WB, Soejima Y, Caner B, Zhang JH (2013) Early brain injury, an evolving frontier in subarachnoid hemorrhage research. Transl Stroke Res 4(4):432–446. doi:10.1007/s12975-013-0257-2
27. Cahill J, Calvert JW, Zhang JH (2006) Mechanisms of early brain injury after subarachnoid hemorrhage. J Cereb Blood Flow Metab: Off J Int Soc Cereb Blood Flow Metab 26(11):1341–1353. doi:10.1038/sj.jcbfm.9600283
28. Yuksel S, Tosun YB, Cahill J, Solaroglu I (2012) Early brain injury following aneurysmal subarachnoid hemorrhage: emphasis on cellular apoptosis. Turk Neurosurg 22(5):529–533. doi:10.5137/1019-5149.JTN.5731-12.1
29. McCormack D, McFadden D (2013) A review of pterostilbene antioxidant activity and disease modification. Oxidative Med Cell Longev 2013:575482. doi:10.1155/2013/575482
30. Kasiotis KM, Pratsinis H, Kletsas D, Haroutounian SA (2013) Resveratrol and related stilbenes: their anti-aging and anti-angiogenic properties. Food Chem Toxicol: Int J Publ Br Ind Biol Res Assoc 61:112–120. doi:10.1016/j.fct.2013.03.038
31. Poulose SM, Thangthaeng N, Miller MG, Shukitt-Hale B (2015) Effects of pterostilbene and resveratrol on brain and behavior. Neurochem Int 89:227–233. doi:10.1016/j.neuint.2015.07.017
32. Rimando AM, Cuendet M, Desmarchelier C, Mehta RG, Pezzuto JM, Duke SO (2002) Cancer chemopreventive and antioxidant activities of pterostilbene, a naturally occurring analogue of resveratrol. J Agric Food Chem 50(12):3453–3457
33. Sies H (2010) Polyphenols and health: update and perspectives. Arch Biochem Biophys 501(1):2–5. doi:10.1016/j.abb.2010.04.006
34. Stevenson DE, Hurst RD (2007) Polyphenolic phytochemicals—just antioxidants or much more? Cell Mol Life Sci: CMLS 64(22):2900–2916. doi:10.1007/s00018-007-7237-1
35. Chiou YS, Tsai ML, Wang YJ, Cheng AC, Lai WM, Badmaev V, Ho CT, Pan MH (2010) Pterostilbene inhibits colorectal aberrant crypt foci (ACF) and colon carcinogenesis via suppression of multiple signal transduction pathways in azoxymethane-treated mice. J Agric Food Chem 58(15):8833–8841. doi:10.1021/jf101571z
36. Wang W, Ding XQ, Gu TT, Song L, Li JM, Xue QC, Kong LD (2015) Pterostilbene and allopurinol reduce fructose-induced podocyte oxidative stress and inflammation via microRNA-377. Free Radic Biol Med 83:214–226. doi:10.1016/j.freeradbiomed.2015.02.029
37. Cairns B, Kim JY, Tang XN, Yenari MA (2012) NOX inhibitors as a therapeutic strategy for stroke and neurodegenerative disease. Curr Drug Targets 13(2):199–206
38. Konior A, Schramm A, Czesnikiewicz-Guzik M, Guzik TJ (2014) NADPH oxidases in vascular pathology. Antioxid Redox Signal 20(17):2794–2814. doi:10.1089/ars.2013.5607
39. Leto TL, Morand S, Hurt D, Ueyama T (2009) Targeting and regulation of reactive oxygen species generation by Nox Family NADPH oxidases. Antioxid Redox Signal 11(10):2607–2619. doi:10.1089/ARS.2009.2637
40. Zhang ZY, Sun BL, Yang MF, Li DW, Fang J, Zhang S (2015) Carnosine attenuates early brain injury through its antioxidative and anti-apoptotic effects in a rat experimental subarachnoid hemorrhage model. Cell Mol Neurobiol 35(2):147–157. doi:10.1007/s10571-014-0106-1
41. Witherell HL, Hiatt RA, Replogle M, Parsonnet J (1998) Helicobacter pylori infection and urinary excretion of 8-hydroxy-2-deoxyguanosine, an oxidative DNA adduct. Cancer Epidemiol Biomark Prev: Publ Am Assoc Cancer Res Cosponsored Am Soc Prev Oncol 7(2):91–96
42. Ayer R, Chen W, Sugawara T, Suzuki H, Zhang JH (2010) Role of gap junctions in early brain injury following subarachnoid hemorrhage. Brain Res 1315:150–158. doi:10.1016/j.brainres.2009.12.016
43. Ayer R, Jadhav V, Sugawara T, Zhang JH (2011) The neuroprotective effects of cyclooxygenase-2 inhibition in a mouse model of aneurysmal subarachnoid hemorrhage. Acta Neurochir Suppl 111:145–149. doi:10.1007/978-3-7091-0693-8_24
44. Moraes L, Grille S, Morelli P, Mila R, Trias N, Brugnini A, N LL, Biestro A, Lens D (2015) Immune cells subpopulations in cerebrospinal fluid and peripheral blood of patients with aneurysmal subarachnoid hemorrhage. SpringerPlus 4:195. doi:10.1186/s40064-015-0970-2
45. Yang F, Wang Z, Wei X, Han H, Meng X, Zhang Y, Shi W, Li F, Xin T, Pang Q, Yi F (2014) NLRP3 deficiency ameliorates neurovascular damage in experimental ischemic stroke. J Cereb Blood Flow Metab: Off J Int Soc Cereb Blood Flow Metab 34(4):660–667. doi:10.1038/jcbfm.2013.242
46. Ma Q, Chen S, Hu Q, Feng H, Zhang JH, Tang J (2014) NLRP3 inflammasome contributes to inflammation after intracerebral hemorrhage. Ann Neurol 75(2):209–219. doi:10.1002/ana.24070
47. Liu HD, Li W, Chen ZR, Hu YC, Zhang DD, Shen W, Zhou ML, Zhu L, Hang CH (2013) Expression of the NLRP3 inflammasome in cerebral cortex after traumatic brain injury in a rat model.

Neurochem Res 38(10):2072–2083. doi:10.1007/s11064-013-1115-z
48. Hoegen T, Tremel N, Klein M, Angele B, Wagner H, Kirschning C, Pfister HW, Fontana A, Hammerschmidt S, Koedel U (2011) The NLRP3 inflammasome contributes to brain injury in pneumococcal meningitis and is activated through ATP-dependent lysosomal cathepsin B release. J Immunol 187(10):5440–5451. doi:10.4049/jimmunol.1100790
49. Jo EK, Kim JK, Shin DM, Sasakawa C (2016) Molecular mechanisms regulating NLRP3 inflammasome activation. Cell Mol Immunol 13(2):148–159. doi:10.1038/cmi.2015.95
50. Denes A, Coutts G, Lenart N, Cruickshank SM, Pelegrin P, Skinner J, Rothwell N, Allan SM, Brough D (2015) AIM2 and NLRC4 inflammasomes contribute with ASC to acute brain injury independently of NLRP3. Proc Natl Acad Sci U S A 112(13):4050–4055. doi:10.1073/pnas.1419090112
51. Sutterwala FS, Haasken S, Cassel SL (2014) Mechanism of NLRP3 inflammasome activation. Ann N Y Acad Sci 1319:82–95. doi:10.1111/nyas.12458
52. Fann DY, Lee SY, Manzanero S, Tang SC, Gelderblom M, Chunduri P, Bernreuther C, Glatzel M, Cheng YL, Thundyil J, Widiapradja A, Lok KZ, Foo SL, Wang YC, Li YI, Drummond GR, Basta M, Magnus T, Jo DG, Mattson MP, Sobey CG, Arumugam TV (2013) Intravenous immunoglobulin suppresses NLRP1 and NLRP3 inflammasome-mediated neuronal death in ischemic stroke. Cell Death Dis 4:e790. doi:10.1038/cddis.2013.326
53. Abais JM, Xia M, Zhang Y, Boini KM, Li PL (2015) Redox regulation of NLRP3 inflammasomes: ROS as trigger or effector? Antioxid Redox Signal 22(13):1111–1129. doi:10.1089/ars.2014.5994
54. Zhang X, Zhang JH, Chen XY, Hu QH, Wang MX, Jin R, Zhang QY, Wang W, Wang R, Kang LL, Li JS, Li M, Pan Y, Huang JJ, Kong LD (2015) Reactive oxygen species-induced TXNIP drives fructose-mediated hepatic inflammation and lipid accumulation through NLRP3 inflammasome activation. Antioxid Redox Signal 22(10):848–870. doi:10.1089/ars.2014.5868
55. Elliott EI, Sutterwala FS (2015) Initiation and perpetuation of NLRP3 inflammasome activation and assembly. Immunol Rev 265(1):35–52. doi:10.1111/imr.12286
56. Li J, Chen J, Mo H, Chen J, Qian C, Yan F, Gu C, Hu Q, Wang L, Chen G (2016) Minocycline protects against NLRP3 inflammasome-induced inflammation and P53-associated apoptosis in early brain injury after subarachnoid hemorrhage. Mol Neurobiol 53(4):2668–2678. doi:10.1007/s12035-015-9318-8
57. Katsnelson MA, Lozada-Soto KM, Russo HM, Miller BA, Dubyak GR (2016) NLRP3 inflammasome signaling is activated by low-level lysosome disruption but inhibited by extensive lysosome disruption: roles for K+ efflux and Ca2+ influx. Am J Physiol Cell Physiol 311(1):C83–C100. doi:10.1152/ajpcell.00298.2015
58. Watters O, O Connor JJ (2011) A role for tumor necrosis factor-alpha in ischemia and ischemic preconditioning. J Neuroinflammation 8:87. doi:10.1186/1742-2094-8-87
59. Verma G, Bhatia H, Datta M (2013) JNK1/2 regulates ER-mitochondrial Ca2+ cross-talk during IL-1beta-mediated cell death in RINm5F and human primary beta-cells. Mol Biol Cell 24(12):2058–2071. doi:10.1091/mbc.E12-12-0885
60. Nakka VP, Gusain A, Mehta SL, Raghubir R (2008) Molecular mechanisms of apoptosis in cerebral ischemia: multiple neuroprotective opportunities. Mol Neurobiol 37(1):7–38. doi:10.1007/s12035-007-8013-9
61. Li T, Liu H, Xue H, Zhang J, Han X, Yan S, Bo S, Liu S, Yuan L, Deng L, Li G, Wang Z (2016) Neuroprotective effects of hydrogen sulfide against early brain injury and secondary cognitive deficits following subarachnoid hemorrhage. Brain Pathol. doi:10.1111/bpa.12361
62. Luna-Vargas MP, Chipuk JE (2016) Physiological and pharmacological control of BAK, BAX, and beyond. Trends Cell Biol. doi:10.1016/j.tcb.2016.07.002
63. Suzuki M, Youle RJ, Tjandra N (2000) Structure of Bax: coregulation of dimer formation and intracellular localization. Cell 103(4):645–654
64. Zhang Z, Lapolla SM, Annis MG, Truscott M, Roberts GJ, Miao Y, Shao Y, Tan C, Peng J, Johnson AE, Zhang XC, Andrews DW, Lin J (2004) Bcl-2 homodimerization involves two distinct binding surfaces, a topographic arrangement that provides an effective mechanism for Bcl-2 to capture activated Bax. J Biol Chem 279(42):43920–43928. doi:10.1074/jbc.M406412200
65. Engel T, Plesnila N, Prehn JH, Henshall DC (2011) In vivo contributions of BH3-only proteins to neuronal death following seizures, ischemia, and traumatic brain injury. J Cereb Blood Flow Metab: Official J Int Soc Cereb Blood Flow Metab 31(5):1196–1210. doi:10.1038/jcbfm.2011.26
66. Chong SJ, Low IC, Pervaiz S (2014) Mitochondrial ROS and involvement of Bcl-2 as a mitochondrial ROS regulator. Mitochondrion 19:39–48. doi:10.1016/j.mito.2014.06.002
67. Jemmerson R, Dubinsky JM, Brustovetsky N (2005) Cytochrome C release from CNS mitochondria and potential for clinical intervention in apoptosis-mediated CNS diseases. Antioxid Redox Signal 7(9–10):1158–1172. doi:10.1089/ars.2005.7.1158
68. Jang JH, Surh YJ (2003) Potentiation of cellular antioxidant capacity by Bcl-2: implications for its antiapoptotic function. Biochem Pharmacol 66(8):1371–1379
69. Zhou XM, Zhou ML, Zhang XS, Zhuang Z, Li T, Shi JX, Zhang X (2014) Resveratrol prevents neuronal apoptosis in an early brain injury model. J Surg Res 189(1):159–165. doi:10.1016/j.jss.2014.01.062
70. Hao XK, Wu W, Wang CX, Xie GB, Li T, Wu HM, Huang LT, Zhou ML, Hang CH, Shi JX (2014) Ghrelin alleviates early brain injury after subarachnoid hemorrhage via the PI3K/Akt signaling pathway. Brain Res 1587:15–22. doi:10.1016/j.brainres.2014.08.069
71. Connolly ES Jr, Rabinstein AA, Carhuapoma JR, Derdeyn CP, Dion J, Higashida RT, Hoh BL, Kirkness CJ, Naidech AM, Ogilvy CS, Patel AB, Thompson BG, Vespa P, American Heart Association Stroke Council, Council on Cardiovascular Radiology and Intervention, Council on Cardiovascular Nursing, Council on Cardiovascular Surgery and Anesthesia, Council on Clinical Cardiology (2012) Guidelines for the management of aneurysmal subarachnoid hemorrhage: a guideline for healthcare professionals from the American Heart Association/American Stroke Association. Stroke: J Cereb Circ 43(6):1711–1737. doi:10.1161/STR.0b013e3182587839
72. Behrouz R, Sadat-Hosseiny Z (2015) Pharmacological agents in aneurysmal subarachnoid hemorrhage: successes and failures. Clin Neuropharmacol 38(3):104–108. doi:10.1097/WNF.0000000000000085